Chemistry–A European Journal

Research Article
doi.org/10.1002/chem.202500095

Chemistry Europe
European Chemical Societies Publishing

www.chemeurj.org

Hydride Rebound: A Frustrated Lewis Pair (FLP)-Type Cooperative Mechanism for H_2 Activation by a Potassium Aluminyl Compound

Keelan M. Byrne,[a] Jamie Hicks,[b] Liam P. Griffin,[b] Simon Aldridge,*[b] and Tobias Krämer*[a, c, d]

Combining experiment and theory, the mechanisms of H_2 activation by the potassium-bridged aluminyl dimer $K_2[Al(NON)]_2$ (NON = 4,5-bis(2,6-diisopropylanilido)-2,7-di-tertbutyl-9,9-dimethylxanthene) and its monomeric K^+-sequestered counterpart have been investigated. These systems show diverging reactivity towards the activation of dihydrogen, with the dimeric species undergoing formal oxidative addition of H_2 at each Al centre under ambient conditions, and the monomer proving to be inert to dihydrogen addition. Noting that this K^+ dependence is inconsistent with classical models of single-centre reactivity for carbene-like Al(I) species, we rationalize these observations instead by a cooperative frustrated Lewis pair (FLP)-type mechanism (for the dimer) in which the aluminium centre acts as the Lewis base and the K^+ centres as Lewis acids. In contrast to previous theoretical work on this precise system by Schaefer and co-workers, the potassium ions are shown to play explicit roles in stabilizing a nascent μ_2-bridging hydride, formed by heterolytic H–H bond cleavage (with accompanying protonation of the aluminium-centred lone pair). K-to-Al hydride "rebound" into the vacant aluminium-centred p-orbital then completes the net addition of H_2 via sequential H^+/H^- transfer. The experimentally determined kinetic isotope effect ($k_H/k_D = 2.6$) reflects a high degree of bond activation in the transition state (as predicted quantum chemically).

Introduction

The activation of dihydrogen is a reaction of critical synthetic utility, not least because of the value associated with numerous (catalytic) industrial hydrogenation processes.[1] It is also a key benchmarking/probe reaction for non-transition metal systems offering novel approaches for the activation of small molecules.[2] Electronically, a key design strategy for such systems involves the manipulation of frontier orbital design/symmetries and energies to mimic patterns established for *d*-block systems (Figure 1a).[2,3] The synergistic mechanism for H–H cleavage involves transfer of electron density *from* the bonding orbital, and *into* its anti-bonding counterpart. Isolobal analogies of this sort have been invoked to rationalize the activation of H_2 by dimetallynes (Figure 1b),[4] by carbenes (and their metallylene analogues; Figure 1c),[5] and to some extent by two-component frustrated Lewis pairs (FLPs; Figure 1d).[6]

Within this sphere, the activation of E–H bonds (E = H, B, C, N, etc.) by aluminium(I) analogues of carbenes, such as {HC(MeCDippN)$_2$}Al (Nacnac^{Dipp}Al, where Dipp = 2,6-^{i}Pr$_2$C$_6$H$_3$),[7] has been the subject of significant research effort.[8] More recently, the advent of aluminyl compounds of the type $[AlX_2]^-$ has opened up additional modes of reactivity - such as the formal oxidative addition of the C–H bond in benzene - based on the more nucleophilic nature of anionic systems of this type.[9–11] Moreover, significant modulation of reactivity is observed depending on the nature of the interaction with the counter-cation. Dimeric system **Al$_D$** (Figure 2), for example, undergoes insertion into the C–H bond of benzene,[9,12] while its monomeric counterpart **Al$_M$** (formed in the presence of 2.2.2-cryptand) inserts into the C–C bond.[13]

In this respect, the differential reactivity observed for the potassium-bridged dimer **Al$_D$** and monomeric K^+-sequestered system **Al$_M$** is potentially informative about the mechanism of dihydrogen activation by aluminyl compounds. This is particularly interesting in light of the mounting evidence from experimental studies for the intervention of alkali cations in chemical transformations.[14] **Al$_D$** undergoes formal oxidative addition of H_2 at each Al(I) centre to give the dimeric dihydroaluminate system **Al$_D$-2H$_2$** over a period of ca. 5 days in benzene solution at room temperature, while **Al$_M$** (as the $[K(2.2.2\text{-crypt})]^+$ salt)[13] is inert to dihydrogen under similar conditions (Figure 2). With this observation in mind, we were keen to probe by

[a] K. M. Byrne, T. Krämer
Department of Chemistry, Maynooth University, Maynooth, Co. Kildare, Ireland

[b] J. Hicks, L. P. Griffin, S. Aldridge
Inorganic Chemistry Laboratory, Department of Chemistry, University of Oxford, South Parks Road, Oxford OX1 3QR, United Kingdom
E-mail: simon.aldridge@chem.ox.ac.uk

[c] T. Krämer
Hamilton Institute, Maynooth University, Maynooth, Co. Kildare, Ireland

[d] T. Krämer
School of Chemistry, Trinity College Dublin, College Green, Dublin, Ireland
E-mail: kraemert@tcd.ie

Supporting information for this article is available on the WWW under https://doi.org/10.1002/chem.202500095

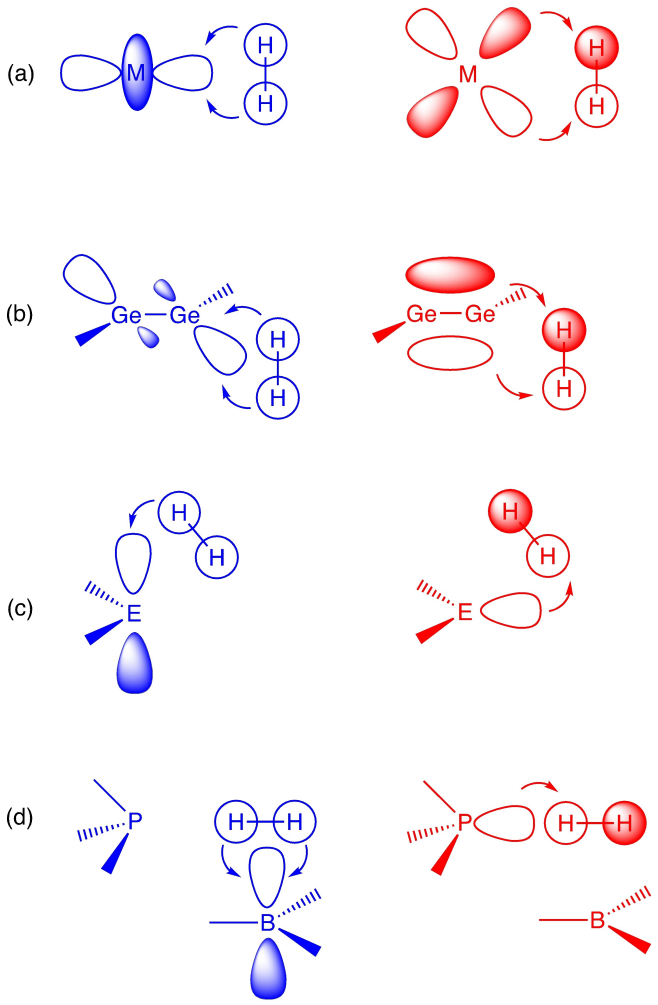

Figure 1. Schematic representation of key orbital interactions in the activation of H_2 by selected one- and two-component systems. Colour scheme: blue - donation from H–H σ bonding orbital; red - 'back-bonding' into H–H σ* anti-bonding orbital.

quantum chemical methods the mechanism(s) for H_2 activation by $\mathbf{Al_D}$ and $\mathbf{Al_M}$ (Figure 3), noting that the apparent K^+ dependency does not fit with classical models of single centre reactivity for carbene-like species, or (more specifically) with the mechanism calculated for this precise system by Schaefer and co-workers.[15]

Given that the conclusions of the present study directly contradict the theoretical results of this earlier study, we first present a brief review of its key results and conclusions. The Schaefer group employed a truncated model of the xanthene-based ligand, in which the ^{i}Pr and ^{t}Bu groups were replaced by methyl groups. This approach was justified through (unpublished) benchmark studies that demonstrated that these substituents have little influence on the interaction of the aluminyl complex with the small and unpolarised H_2 molecule. Based on our own comprehensive benchmark calculations (see ESI), such truncations are fully justified and lead to a significant speed-up of the calculations without loss of accuracy. The Schaefer team employed the M06-2X/def2-SVP level of theory to optimise molecular geometries and perform frequency calculations, owing to the size of the dimeric complex $\mathbf{Al_D}$; even the truncated system is composed of a sizable 228 atoms, 796 electrons and 2104 basis functions. Accurate single-point energies were obtained from high-level DLPNO-CCSD(T)/def2-TZVP computations. The transition state for H_2 activation located for the monomeric complex $\mathbf{Al_M}$ ($\mathbf{TS_M}$, Figure 4) revealed a side-on approach of H_2 to the aluminyl anion, following a trajectory approximately perpendicular to the N–O–N plane. The three-centred transition state is characterised by high asynchronicity in the Al–H bond formation, with one bond almost formed (Al–H1 1.63 Å) and the other halfway completed (Al–H2 2.14 Å). Following the intrinsic reaction coordinate from $\mathbf{TS_M}$ towards the product, it was shown that H1 follows a C-shaped trajectory towards the final Al–H formation.[16] Natural Population Analysis (NPA) charges indicate significant polarisation of the H_2 molecule, with the charge on the more protic H1 atom decreasing more slowly (compared to the more hydridic H2 atom) upon approaching the transition state due to the primary formation of the Al–H1 bond. In parallel, the charge on the Al centre increases until the product is reached, in agreement with a two-electron oxidative addition mechanism. Such a transition state is highly reminiscent of that for oxidative addition of dihydrogen to the silylene compound Si{B(NDippCH)$_2$}{N(SiMe$_3$)Dipp},[17] and implies electrophilic activation of H_2 primarily via donation of electron density from the H_2 σ-orbital into the empty Al p-orbital. We note that in the case of aluminyl species the demarcation of electrophilic and nucleophilic activation is less clear cut than for carbenes due to the more diffuse character of the Al lone pair, but we nonetheless

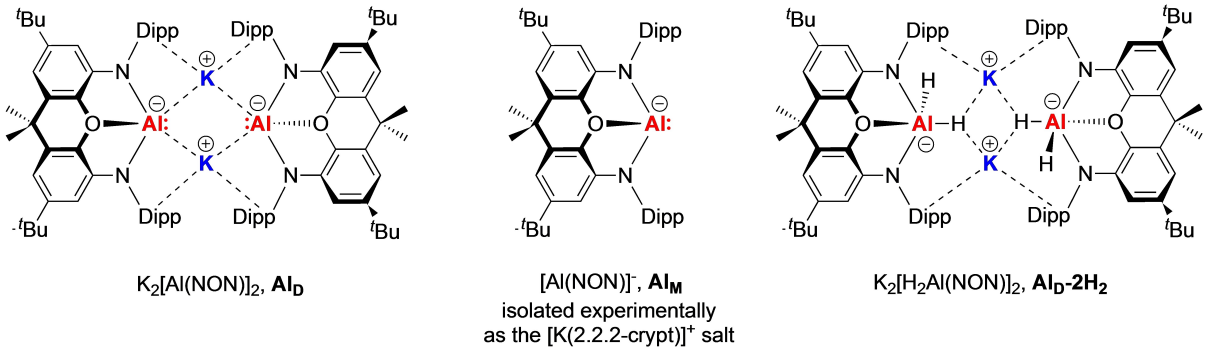

Figure 2. Aluminyl compounds of relevance to the current study.

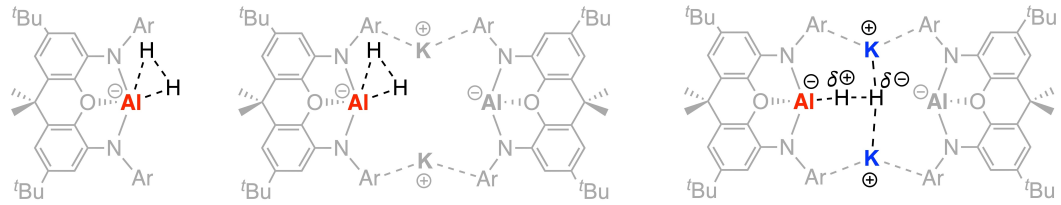

Figure 3. Possible transition states along H_2 activation pathways in Al_M and Al_D.

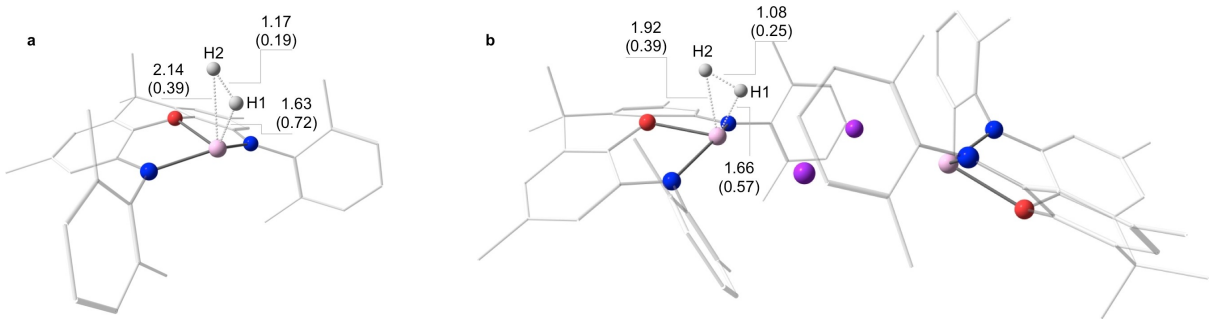

Figure 4. Optimized geometries (M06-2X/def2-SVP) of (a) TS_M and (b) TS_D-I reported by Schaefer and co-workers along with bond distances (in Å) and Mayer Bond Indices (in parentheses). Figure reproduced from data in reference [15].

utilise this terminology to distinguish between these two alternatives.

Schaefer *et al.* found that the transition states for the consecutive activation of two H_2 molecules by the contacted dimer pair Al_D were both structurally and energetically similar to TS_M. Bond parameters and charge distributions, together with the H_2 trajectory support the notion of *electrophilic* activation of H_2 (TS_D-I associated with the first addition is shown for comparison in Figure 4), although the authors themselves imply a *nucleophilic* activation mechanism. The calculated Gibbs activation energies $\Delta G_{298}^{\ddagger}$ are very close to one another for both the monomeric and dimeric systems. The slightly higher barrier associated with TS_M ($\Delta G_{298}^{\ddagger} = 30.7$ kcal mol^{-1}) compared to TS_D-I and TS_D-II ($\Delta G_{298}^{\ddagger} = 29.7$ and 29.6 kcal mol^{-1}) was insignificant to attribute this to a cooperative effect by the K^+ ions. Importantly, Schaefer and co-workers state that "all attempts to locate a suitable transition state corresponding to a frustrated Lewis pair (FLP)-type pathway, in which the H_2 molecule would be activated between the basic Al and an acidic K^+ site were unsuccessful". This interesting possibility for a cooperative mechanism in which the K^+ ions are actively involved in the H_2 activation process in this particular system was previously speculated on by Hinz and Breher in a highlight article,[18] and the authentication of such a transition state would mark a significant departure from the current mechanistic paradigm pertaining to H_2 activation in these and related systems. In their study, Schaefer an co-workers conclude that "all these energetic features let us conjecture that K^+ atoms do not exert a crucial catalytic role in the activation of the non-polar H_2 molecule, even in cooperation with the monomer complexes." By contrast, in the study outlined below we will present experimental and theoretical results that indeed corroborate a FLP-type deprotonation mechanism for H_2 activation by dimeric Al_D.

Results and Discussion

To interrogate the mechanistic details associated with H_2 activation by Al_M and Al_D, we utilised quantum chemical calculations. We employed the same truncation in our structural model as Schaefer *et al.*, i.e. replacing ^{i}Pr and ^{t}Bu groups of the NON ligand by methyl groups. Gas phase geometry optimizations and frequency calculations of all species were performed at the TPSS/def2-SVP level of theory, based on the overall good performance of this meta-GGA functional in generating structures that compare well with experimental data.[19,20] We found that the D3 dispersion correction led to some over-binding and contraction of the contacted dimer pair in Al_D but had negligible effect on the geometry of the monomeric Al_M species, and hence this correction was not considered for geometry optimisations. Similar protocols omitting D3 have been reported in the literature for related systems.[14c,d] With this approach and in combination with the def2-SVP basis set, the bond parameters of the optimized geometries reproduce those of their crystallographic counterparts with very good accuracy (see Table S2), whereas utilisation of a def2-TZVP basis set did not offer any notable improvement. Moreover, we confirmed that all electrons were bound to the molecules by careful inspection of the frontier molecular orbitals. Single point energies were calculated with the M06-2X functional in combination with the D3 dispersion correction, a larger def2-

TZVPP basis set and a polarisable continuum model to account for the effects of benzene solvent. This theoretical approach including the above approximations was validated by comprehensive benchmark calculations comparing different methods on the truncated and full systems, converging to very similar results in all cases (see Tables S2 and S3 as well as Figures S13–S19). We emphasise that our results are fully reproducible at the same level of theory employed by Schaefer's group and note that our conclusions are largely insensitive to any particular choice of level of theory (including dispersion and solvation corrections). In the following discussion, we report results obtained at the SMD(benzene)-M06-2X–D3/def2-TZVPP//TPSS/def2-SVP level of theory.

The reaction energy profile for the addition of H_2 to the anionic aluminyl monomer, $\mathbf{Al_M}$, is shown in Figure 5. Initial approach of H_2 to $\mathbf{Al_M}$ gives the reactant encounter complex $\mathbf{Al_M + H_2}$, a process which is slightly endergonic (ΔG_{298} = 3.1 kcal mol^{-1}). The ensuing transition state $\mathbf{TS_M}$ has an overall calculated barrier of $\Delta G_{298}^{\ddagger}$ = 31.6 kcal mol^{-1}, whilst the reaction energy to formation the Al(III) dihydride species $\mathbf{Al_M\text{-}H_2}$ is strongly exergonic (ΔG_{298} = −35.4 kcal mol^{-1}).

These values compare well with those reported by Schaefer *et al.* (e.g. $\Delta G_{298}^{\ddagger}$ = 30.7 kcal mol^{-1} from DLPNO-CCSD(T)/def2-TZVP//M06-2X/def2-SVP. Reassuringly, these energies also show excellent agreement to our own DLPNO-CCSD(T)/def2-TZVP energies (on TPSS/def2-SVP geometries), yielding $\Delta G_{298}^{\ddagger}$ = 32.3 kcal mol^{-1} and ΔG_{298} = −35.3 kcal mol^{-1} (Table S3, Figures S13 and S14). The high activation barrier for this process is in line with literature reports and agrees with the observation that the 'naked' aluminyl anion is unable to activate H_2 under ambient conditions (298 K, 1 atm H_2).[8b] The corresponding geometry of the $\mathbf{TS_M}$ is characteristic of a three-membered concerted oxidative addition of H_2 to the Al centre and its asynchronous nature is again evident from the asymmetric Al–H1 (1.64 Å) and Al–H2 (1.97 Å) bond distances. The H–H distance (1.16 Å) in $\mathbf{TS_M}$ indicates appreciable activation of this bond (Figure 6).

In contrast to the transition state for electrophilic activation of H_2 discussed by Schaefer and co-workers, in this $\mathbf{TS_M}$ the H_2 molecule approaches the Al lone pair from within the equatorial plane, reminiscent of the *nucleophilic* H_2 activation mechanism at Nacnac^{Dipp}Al and cyclic (alkyl)(amino)carbenes.[5,21] Although this pathway is somewhat more favorable than the alternative electrophilic activation (see Figures S13 and S14), this is a minor point that does not affect the further discussion and merely reflects the higher nucleophilicity of the Al centres in the xanthene-based system. Analogous to the report by Schaefer and co-workers, the NPA charges on the H_2 fragment in $\mathbf{TS_M}$ indicate a degree of polarization of the molecule, with −159 and −261 milli-electrons located on H1 and H2, respectively. These decrease towards approximately −440 milli-electrons on both hydrogens in the product. As expected for an oxidative

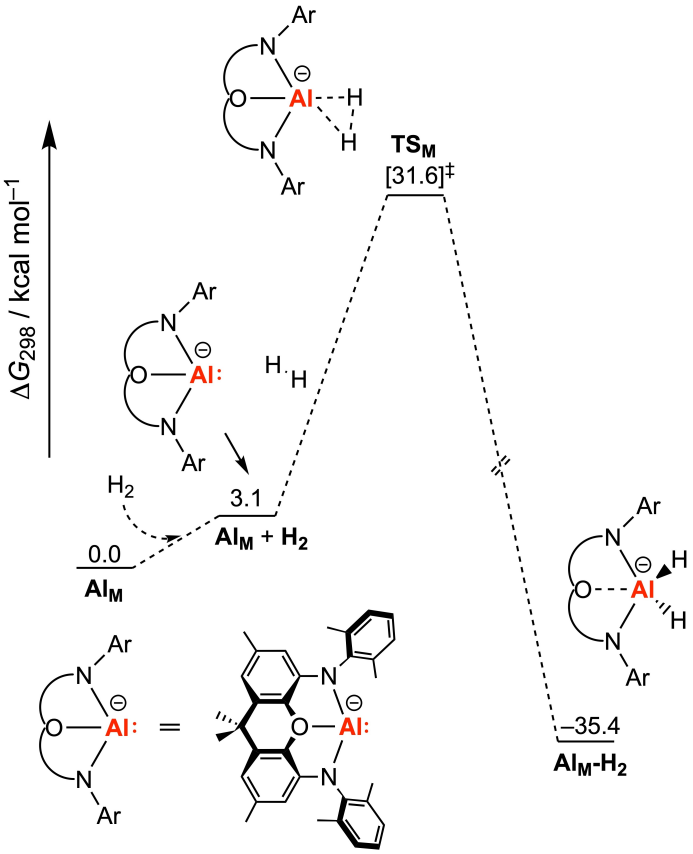

Figure 5. Gibbs Free Energy profile for activation of H_2 by the anionic aluminyl monomer $\mathbf{Al_M}$, calculated at the SMD(benzene)-M06-2X–D3/def2-TZVPP//TPSS/def2-SVP level of theory.

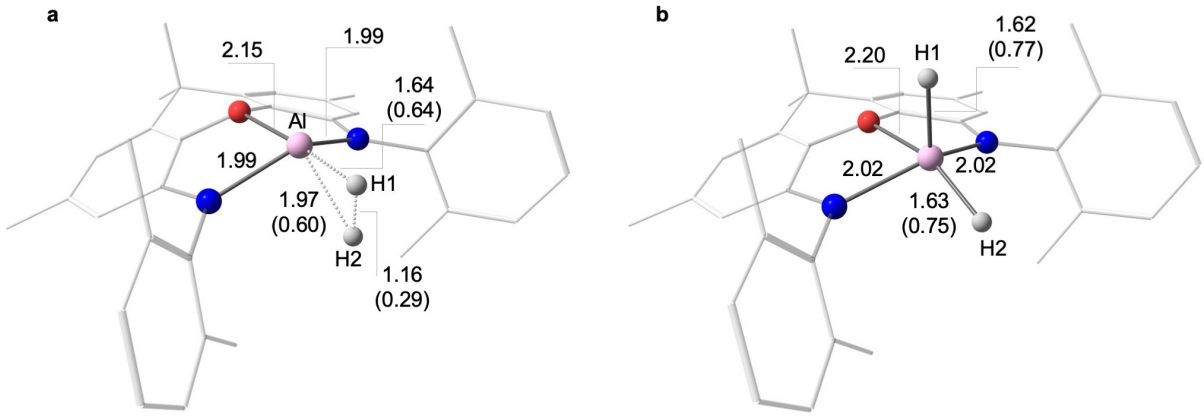

Figure 6. Optimized geometries (TPSS/def2-SVP) of (a) $\mathbf{TS_M}$ and (b) $\mathbf{Al_M\text{-}H_2}$ along with bond distances (in Å) and Wiberg Bond Indices (in parentheses).

addition process, the charge on the Al centre becomes more positive along the pathway, increasing from +717 milli-electrons in $\mathbf{Al_M}$ to +967 milli-electrons in $\mathbf{TS_M}$, and reaching the final value of +1399 milli-electrons in the product. The analysis of Voronoi charges corroborate the protic and hydridic character of the H1 and H2 atoms, as expected for this interaction (see below). The corresponding Wiberg Bond Indices are 0.60, 0.64 and 0.29 for the Al–H and H–H bonds, respectively. The H–Al–H scissoring mode associated with the eigenvector along the reaction path (i1100 cm^{-1}) reveals the breaking of the H–H bond and formation of two Al–H bonds, with concomitant widening of the H–Al–H angle.[15,21] Unlike in the electrophilic activation mechanism, in this case both H atoms describe an arc-like trajectory (scissoring mode) along the IRC until reaching their final position in the product.

Turning to the addition of dihydrogen to the potassium-stabilized aluminyl contact dimeric pair, $\mathbf{Al_D}$, the activation step associated with the addition of the first H_2 molecule does not proceed via a concerted oxidative addition step but a *new* transition state $\mathbf{TS_D\text{-}I}$, in which H_2 is activated via the cooperative action of the two potassium ions and the Al centre (Figure 7). The H–H stretching mode associated with the eigenvector along the reaction path (i904 cm^{-1}) reveals the breaking of the H–H bond and concomitant formation of an Al–H bond. Relaxed surface scans indicate that $\mathbf{TS_D\text{-}I}$ is the only first order saddle point in this region of the PES. This is further supported by mapping out the minimum energy path (MEP) via the Nudged Elastic Band (NEB) algorithm, which yields the same transition state as optimised above with the conventional eigenvector-following method (see Figure S12).

The optimized geometry of $\mathbf{TS_D\text{-}I}$ reveals that the H_2 unit interacts in an end-on fashion with the Al(I) centre, while adopting a side-on bridging position between both K^+ ions (Figure 8). NPA charges located on H1 (−324 milli-electron) and H2 (−514 milli-electrons) substantiate a slightly more polarized H_2 molecule in $\mathbf{TS_D\text{-}I}$ than in $\mathbf{TS_M}$. These evolve to −457 and −535 milli-electrons in $\mathbf{Al_D\text{-}H_2}$, with the more negative charge on H2 being due to its proximity to both K^+ ions. The charge on aluminium follows the same trend as observed for the monomeric system, but with more notable charge polarisation in $\mathbf{TS_D\text{-}I}$ due to addition of the protic H1 (+0.762 milli-electrons in $\mathbf{Al_D}$, +1396 milli-electrons in $\mathbf{TS_D\text{-}I}$, +1471 milli-electrons in $\mathbf{Al_D\text{-}H_2}$). The H–H bond distance (1.23 Å) and WBI (0.25) signal substantial activation of the H_2 molecule in parallel with a Al1–H1 bond that is already partially formed (1.81 Å, WBI 0.57), geometric parameters that are characteristic of a late transition state. The K···H2 distances are nearly identical (2.50 Å and 2.57 Å) and are indicative of a symmetrical μ_2-H bridging mode. The partial Al1–H1 bond and hydridic character of H2 are also apparent from the natural Lewis structure obtained from NBO analysis of the wavefunction. These features are reminiscent of the FLP-type H_2 activation mechanisms thought to operate for the $[KCH_2C_6H_5]_2$ dimer or a related lithium phosphide proposed by Stephan,[22] in which the Lewis-acidic alkali metals exert a cooperative effect during the activation process (see Figure S11). We note that this mechanism may also be interpreted in terms of a deprotonation reaction observed for organoalkali compounds, such as the hydrogenolysis of LiCCH with H_2,[23] typically involving transition states in which the deprotonating carbanion centre aligns with the H–H axis and the alkali ion interacts side-on with H_2. In the present case the formed alkali hydride ("K_2H") is concomitantly complexed by the Lewis-acidic Al(III) centre. Both descriptions of the new mechanism as either FLP-type or a cooperative deprotonation reaction appear equivalent. Attempts to locate a transition state for (nucleophilic) concerted oxidative activation of H_2 similar to $\mathbf{TS_M}$ within the dimer were unsuccessful, due to immediate re-orientation of the H_2 molecule during the geometry optimisation and convergence to the FLP-type transition state. Tracing the forward IRC from $\mathbf{TS_D\text{-}I}$ towards the first intermediate $\mathbf{Al_D\text{-}H_2}$, the protic hydrogen H1 transfers onto the lone pair of the Al centre to form the Al–H bond, while the K^+ ions capture the hydridic H2 end of H_2 until the proton has moved into its position adopted in the product. Subsequently, the hydride H2 swings around and transfers onto the Al centre ("hydride rebound"). Concomitant with this process, hybridization between the relevant Al s- and p-orbitals occurs (see ESI for details of NBO analysis and animated trajectory for this process).

Addition of the second H_2 molecule at the other aluminium centre occurs via an analogous transition state, with similar

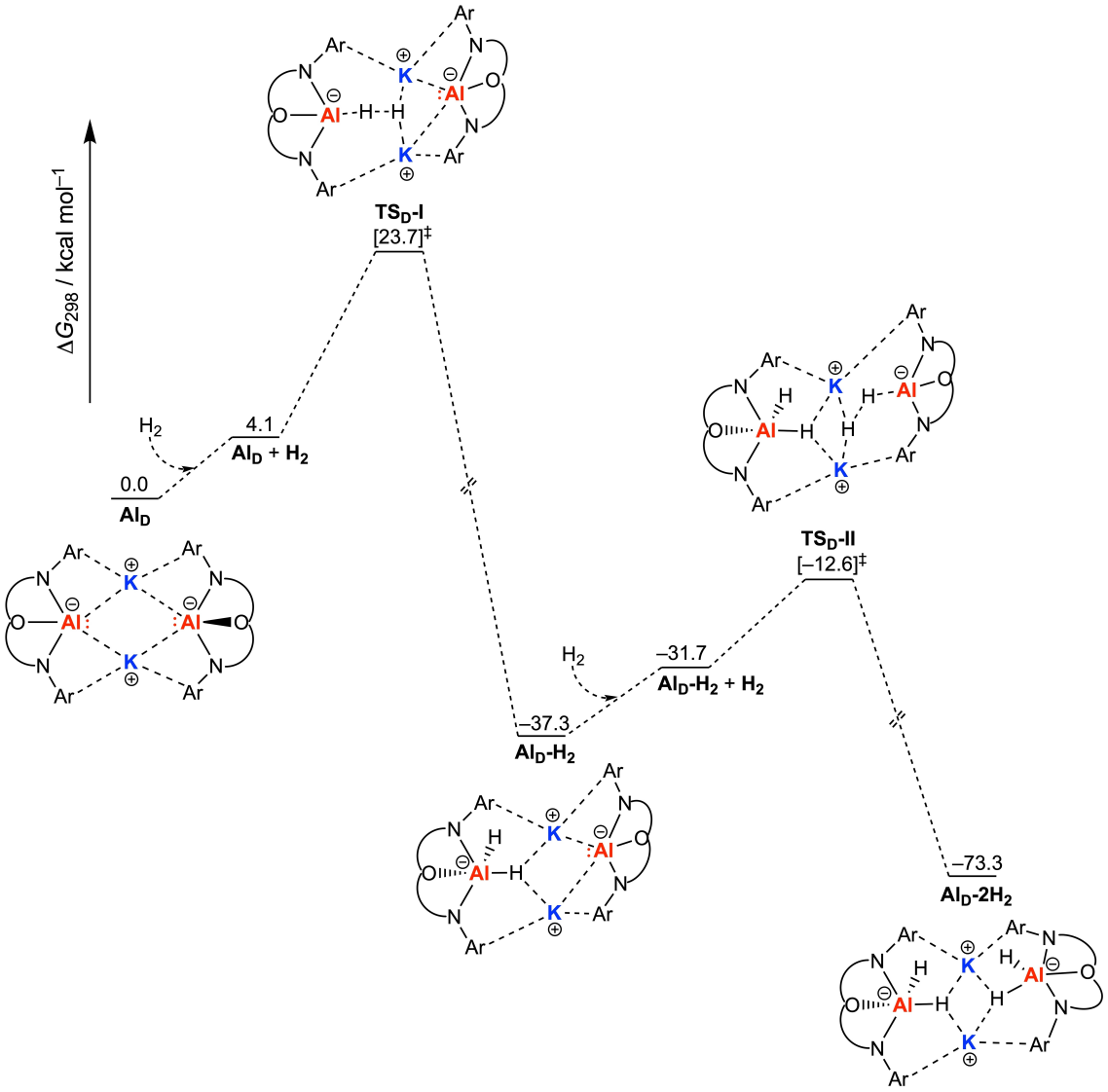

Figure 7. Gibbs Free Energy profile for K^+ mediated activation of H_2 by the aluminyl contacted dimer pair **Al_D**, calculated at the SMD(C_6H_6)-M06-2X–D3/def2-TZVPP//TPSS/def2-SVP level of theory.

structural features and an energetic barrier ($\Delta G_{298}^{\ddagger}$ = 24.7 kcal mol^{-1}) that is only marginally higher than in the first activation step (this difference is insubstantial and within the error of the calculation). It is evident that the cooperative action of both K^+ ions during H_2 activation leads to a significant stabilisation (by 8–9 kcal mol^{-1}) of the new FLP-type transition states relative to the concerted oxidative addition process previously postulated to operate in the aluminyl contacted dimer pair.[15] Calculated activation energies obtained in toluene solvent at T = 328 K are comparable to those reported above (see Figure S16), in excellent agreement with the corresponding experimental values ($\Delta G_{328}^{\ddagger}$ = 25 kcal mol^{-1}) and consistent with the observed reaction time of 5 days at room temperature.

The overall Gibbs Free Energy for successive addition of two equivalents of H_2 to **Al_D** amounts to −73.3 kcal mol^{-1}, furnishing the thermodynamically very stable Al(III) product complex **Al_D-$2H_2$**. The exothermicities of each step are again nearly identical, corresponding to ΔG_{298} = −37.3 kcal mol^{-1} and ΔG_{298} = −36.0 kcal mol^{-1}, respectively. Both processes occur in concerted fashion and lead to the Al(III)H_2 products without further intermediate species, as confirmed by following the IRC in both directions from the transition states (Figure S20). Specifically, intermediates featuring a bridged K(μ_2-H)K motif could not be stabilized during separate geometry optimizations (performed both in vacuum and with a polarisable continuum to account for any potential solvent effects), due to the hydride transferring onto the Lewis-acidic Al(III) centre. It is worth noting that this hydride rebound onto the electrophilic Al centre has some precedent on the macroscopic scale: in the reaction of (NON)AlH with KH, the Lewis-acidic aluminium centre in (NON)AlH takes up hydride to give K[(NON)AlH_2] (see ESI). Collectively, the structural and energetic similarities between the two addition steps preclude any significant allosteric effects, i.e. both aluminyl fragments act effectively independently of

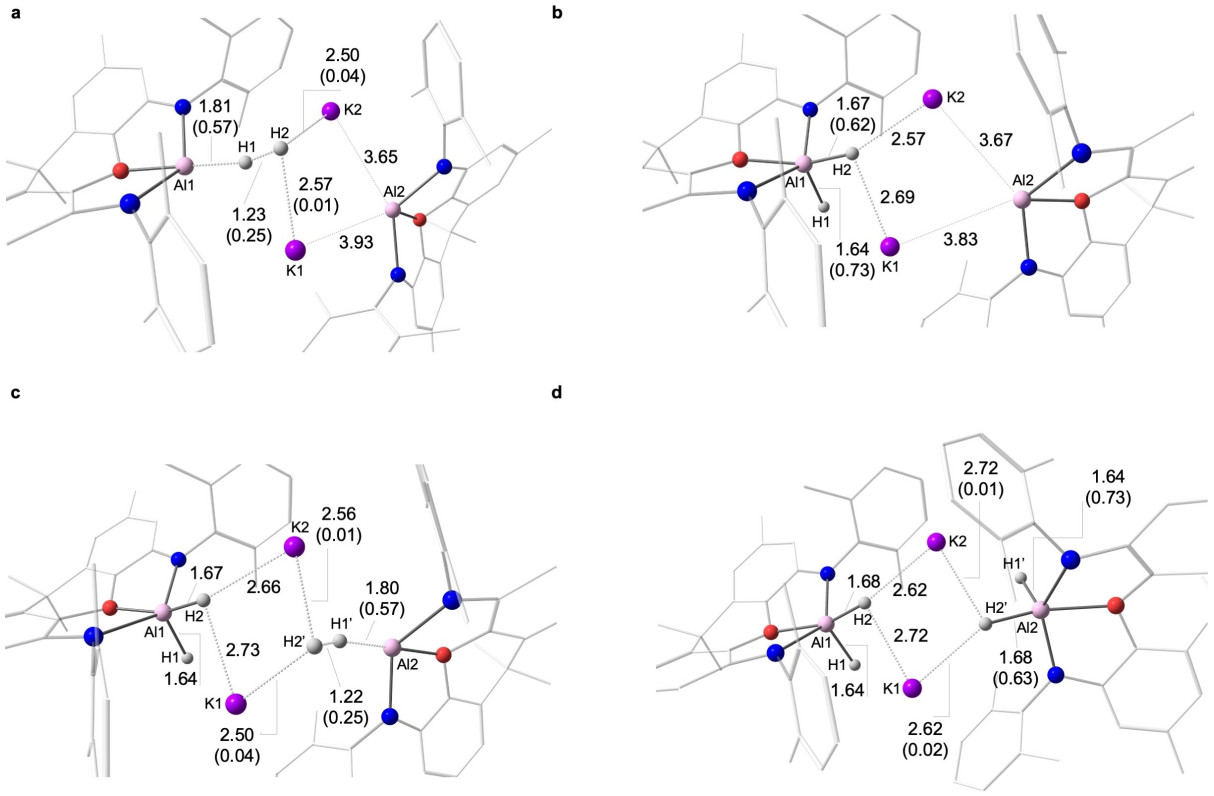

Figure 8. Optimized geometries (TPSS/def2-SVP) of (a) $\mathbf{TS_D\text{-}I}$, (b) $\mathbf{Al_D\text{-}H_2}$, (c) $\mathbf{TS_D\text{-}II}$ and (d) $\mathbf{Al_D\text{-}2H_2}$ along with selected bond distances (Å) and Wiberg Bond Indices (in parentheses).

each other during the reaction, in agreement with the conclusions drawn by Schaefer and co-workers.

The more favourable interaction between H_2 and the aluminyl fragment in this new FLP type mechanism is also borne out in the combined activation strain model/energy decomposition analysis performed at a consistent geometry with a H···H distance of 1.2 Å (coincident with the geometry of $\mathbf{TS_D\text{-}I}$; see ESI for full details and comparison of these data along the reaction coordinate). The computed total strain energy for the FLP-type pathway ($\Delta E_{strain} = 47.1$ kcal mol^{-1}) is slightly higher than for the concerted oxidative addition pathway ($\Delta E_{strain} =$ 45.3 kcal mol^{-1}), due to marginal structural changes in the aluminyl fragment. However, the strain energy in the former is more than compensated by an advantageous interaction between H_2 and the $\mathbf{Al_D}$ fragment, which is substantially more stabilizing ($\Delta E_{int} = -33.5$ kcal mol^{-1}) than that calculated for oxidative addition ($\Delta E_{int} = -25.9$ kcal mol^{-1}). Further decomposition of the interaction energy term reveals that this effect can be mainly attributed to loss of Pauli repulsion in the FLP-type pathway ($\Delta E_{Pauli} = 126.6$ kcal mol^{-1} *vs.* 173.0 kcal mol^{-1}), which is offset by both electrostatic ($\Delta E_{elec} = -43.3$ kcal mol^{-1}) and orbital terms ($\Delta E_{orb} = -113.5$ kcal mol^{-1}). Although the magnitude of both these latter terms at this particular H···H distance are smaller in the FLP-type pathway than for the concerted oxidative addition process, in sum the FLP pathway becomes more favourable. As expected for the H_2 molecule, dispersion effects are similar but small in both pathways. Stabilisation of the Al lone pair in $\mathbf{TS_D\text{-}I}$ by the K^+ ions strengthens back-donation into the H_2 σ^* orbital ($\Delta E_{orb} = -101.0$ kcal mol^{-1}), albeit at the expense of a reduced donation from the H_2 σ orbital into the Al centre ($\Delta E_{orb} = -10.0$ kcal mol^{-1}). Even though on first sight the H_2 molecule adopts a more unfavorable end-on orientation with the Al(I) and K^+ centres in the FLP-type trajectory, stabilizing orbital interactions are maintained. As a result, the *total* orbital terms ($\Delta E_{orb} = -113.5$ kcal mol^{-1}) remain *relatively* close to those for oxidative addition ($\Delta E_{orb} =$ -129.4 kcal mol^{-1}).

This shift in mechanism from concerted oxidative addition for $\mathbf{Al_M}$ towards a (lower barrier) FLP-type H_2 activation with $\mathbf{Al_D}$ directly contrasts the findings by Schaefer *et al.*, and provides a rationale for the experimentally observed change in reactivity (i.e. $\mathbf{Al_D}$ activates H_2 at room temperature, but $\mathbf{Al_M}$ does not). Activation barriers associated with concerted oxidative addition of H_2 (irrespective of an electrophilic or nucleophilic mode) are in any case prohibitively high for a reaction to occur at room temperature. Moreover, the reaction of $\mathbf{Al_D}$ with H_2 is characterized by an experimental primary kinetic isotope effect of $k_H/k_D = 2.6$, (see ESI), consistent with the high degree of heterolytic activation of the H_2 molecule in the corresponding transition state predicted by the quantum chemical calculations. For context, an experimental KIE of 1.5 for the FLP-type activation of H_2 in the presence of NEt_3 as Lewis-base and a Sn(II) Lewis-acid was recently reported by Ashley and co-workers,[24] while Erker and Grimme have reported a KIE of 3.2 for the release of H_2 from an FLP-derived phosphonium borohydride zwitterion.[25]

Analysis of the Voronoi Deformation Densities (VDD) reveals how the bonding interaction between the H_2 and Al fragments modifies the electron density distribution in the transition states. The charge changes $\triangle Q$ represent the amount of electronic charge that flows into ($\triangle Q < 0$) or out of ($\triangle Q > 0$) the Voronoi cell of an atom due to the interaction between the molecular fragments. In case of **TS_M**, the H_2 unit is polarized upon interaction with the metal centre (Figure 9), rendering one hydrogen atom protic (+70 milli-electrons) and the other hydridic (−162 milli-electrons). The heterolytic character stems from the initial attack of the Al(I) lone pair on the σ^*-orbital of H_2 and the transfer of the hydride-like hydrogen into the Al(I) p-orbital to form the Al(III) dihydride species. By comparison, charge separation for the hydridic and protic hydrogens is more pronounced in **TS_D-I**, amounting to −334 and +104 milli-electrons, respectively. This effect can be attributed to a polarisation exerted by the K^+ ions, and correlates with the larger degree of activation of the H–H bond in this transition state. The charge flow for the potassium centres is comparatively small (+26 and +7 milli-electrons), whilst those for the Al ions in both **TS_M** and **TS_D-I** show similar increases of +84 and +61 milli-electrons, as expected for oxidation processes involving the metal centres. The charge analysis for the second addition of H_2, via **TS_D-II** is nearly identical (see Figures S20–S22), and collectively provides further support for the description of these transition states as having FLP-type character.

The presence of weak $K^+\cdots H$ contacts in **TS_D-I** is confirmed by analysis of the topology of the total electron density using the quantum theory of atoms-in-molecules (QTAIM) approach (Figure 10). Bond paths and associated bond critical points (BCPs) are found between the Al, H and K centres involved in the transition states. The parameters of the BCP associated with H2···K1/K2 are consistent with closed-shell electrostatic interactions, as reflected in low values of the electron density ($\rho(r)$~0.015 au), positive Laplacian ($\nabla^2\rho(r) = 0.050$ au) and equal magnitudes of the potential and kinetic energy densities ($|V(r)| = G(r) = 0.01$ au).

Analysis of the parameters of the Al1–H1 BCP corroborate the advanced stage of formation of a covalent bond at the transition state, as evidenced by the value of $\rho(r)$ (+0.061 au), the near-zero value of $\nabla^2\rho(r)$ (+0.003 au), and the negative value of the total energy density $H(r)$ (−0.025 au). The H1–H2

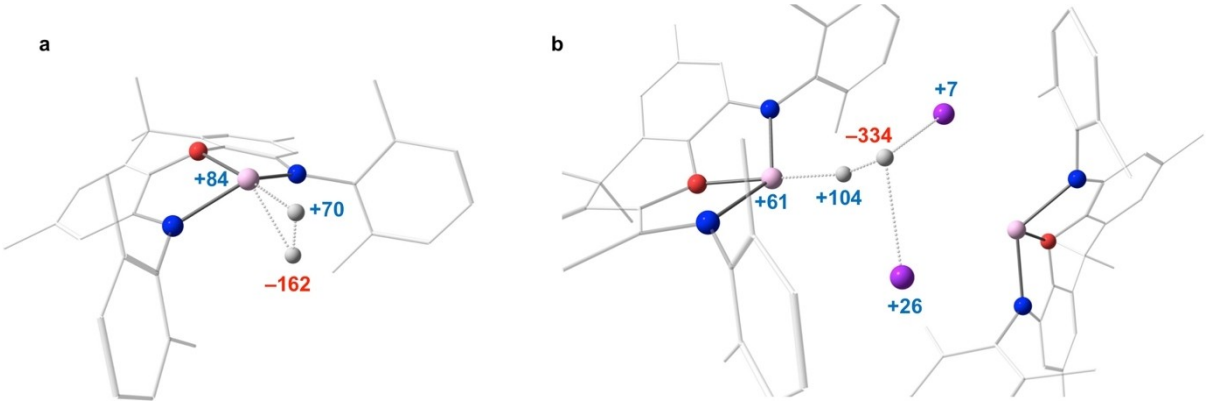

Figure 9. Change in Voronoi Deformation Density (VDD) atomic charge ($\triangle Q$, in milli-electrons) for **a TS_M** and **b TS_D-I** (TPSS/TZ2P).

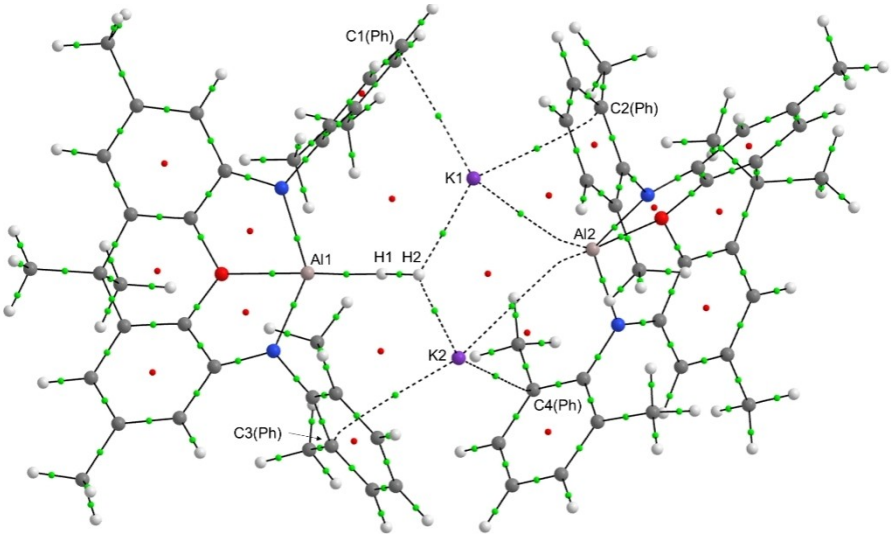

Figure 10. QTAIM molecular graph of **TS_D-I** (M06-2X/def2-TZVPP//TPPS/def2-SVP) with bond critical points (BCP) and ring critical points (RCP) shown as green and red spheres, respectively. Bond paths are shown as solid and dotted lines.

bond is significantly activated at the transition state (more so than in Stephan's $[KCH_2C_6H_5]_2$ dimer) but maintains a non-negligible amount of covalent character (relatively high value of $\rho(r)$, negative value of $\nabla^2\rho(r)$ and a negative $H(r)$). The presence of BCPs and (curved) line paths in the QTAIM topology also confirm the presence and non-covalent nature of long-range alkali $K^+\cdots\eta^6$-arene and $K^+\cdots$Al interactions, having characteristically small values of $\rho(r)$, $\nabla^2\rho(r)$ and local energy densities (see ESI).[25] Ring critical points (RCPs) at the approximate centres of the Al–O–C-C–N units are consistent with the chelating binding mode of the tridentate NON ligand. These QTAIM results are very similar to those reported independently by Schaefer, Coles and Harder.[14,15,27] Similar results are also found for the $K^+\cdots$H contacts in **TS_D-II** as well as the resulting product complexes **Al_D-H_2** and **Al_D-2H_2** (see ESI). In the latter, the bond in H_2 is fully broken and the presence of new Al–H bonds is confirmed by the presence of corresponding bond paths and BCPs, with the separated hydrides further stabilised by $K^+\cdots$H interactions.

In conclusion, combined experimental and theoretical results demonstrate that the activation of H_2 by the $K_2[Al(NON)]_2$ dimer proceeds through a stepwise FLP-type mechanism between basic aluminyl and acidic K^+ sites. Thus, in this mechanism, a single Al(I) centre acts as a Lewis-base donor, while both potassium centres act as Lewis-acid acceptors. In the transition state the polarised H_2 molecule interacts in an end-on fashion with both donor and acceptor functions, and forms a symmetrical μ_2-H bridge between the K^+ ions. H–H cleavage is accompanied by transfer of the protic hydrogen to the lone pair of the Al(I) centre; subsequent "rebound" of the hydride from the K(μ_2-H)K unit exploits the acceptor p-orbital at Al. As such, the K^+ ions are not mere spectators that support the dimeric structure, but instead take an active role in the mechanism of H_2 cleavage, refuting previous studies by Schaefer and co-workers. These authors proposed stepwise electrophilic oxidative addition of H_2 at each Al centre in dimeric **Al_D**, analogous to the mechanism of the monomer, but discarded the possibility of a cooperative (FLP-type) mechanism. This cooperative action of metal centres in an FLP-type mechanism helps to significantly reduce the barrier for the activation process as compared to "traditional" concerted oxidative addition. Moreover, this result is fully consistent with the experimentally observed absence of H_2 activation in the corresponding monomeric system in which the K^+ cation is sequestered by cryptand. This FLP-type mechanism has implications for related alkali-metal supported aluminyl systems (and more broadly for mixed metal bimetallics),[14] and opens new avenues for exploiting alkali metal cooperativity in other E–H bond activation reactions.[28] Work in the Krämer group is currently ongoing to elucidate the effect on the mechanism of variation in the alkali metal and supporting ligand.

Acknowledgements

The authors wish to acknowledge the Irish Centre for High-End Computing (ICHEC) for the provision of computational facilities and support. K.M.B. thanks the Irish Research Council for funding under grant number GOIPG/2022/470. T.K. thanks the RSC for a Research Enablement Grant (E21-7643704122). L.P.G. thanks the EPSRC Centre for Doctoral Training in Inorganic Chemistry for Future Manufacturing (OxICFM; EP/S023828/1) for studentship support.

Conflict of Interests

The authors declare no conflict of interest.

Data Availability Statement

The data that support the findings of this study are available in the supplementary material of this article.

Keywords: Hydrogen activation · Density functional calculations · Aluminium · Frustrated Lewis pair · Alkali metal mediation.

[1] Wiley, Weinheim **2006** *The Handbook of Homogeneous Hydrogenation* Edited by J. G. de Vries, C. J.Elsevier.
[2] P. P. Power, *Nature* **2010**, *463*, 171.
[3] G. J. Kubas, *Metal Dihydrogen and σ-Bond Complexes: Structure, Theory and Reactivity*, Kluwer Academic/Plenum, New York **2001**.
[4] a) G. H. Spikes, J. C. Fettinger, P. P. Power, *J. Am. Chem. Soc.* **2005**, *127*, 12232; b) L. Zhao, F. Huang, G. Lu, Z.-X. Wang, P. von Ragué Schleyer, *J. Am. Chem. Soc.* **2012**, *134*, 8856.
[5] G. D. Frey, V. Lavallo, B. Donnadieu, W. Schoeller, G. Bertrand, *Science* **2007**, *316*, 439.
[6] G. C. Welch, R. R. San Juan, J. D. Masuda, D. W. Stephan, *Science* **2006**, *314*, 1124.
[7] C. Cui, H. W. Roesky, H.-G. Schmidt, M. Noltemeyer, H. Hao, F. Cimpoesu, *Angew. Chem. Int. Ed.* **2000**, *39*, 4274.
[8] a) Y. Lui, J. Li, X. Ma, Z. Yang, H. W. Roesky, *Coord. Chem. Rev.* **2018**, *374*, 387; b) T. Chu, G. I. Nikonov, *Chem. Rev.* **2018**, *118*, 3608; c) G. Coates, F. Rekhroukh, M. Crimmin, *Synlett.* **2019**, *30*, 2233.
[9] J. Hicks, P. Vasko, J. M. Goicoechea, S. Aldridge, *Nature* **2018**, *557*, 92.
[10] a) R. J. Schwamm, M. D. Anker, M. Lein, M. P. Coles, *Angew. Chem. Int. Ed.* **2019**, *58*, 1489; b) S. Kurumada, S. Takamori, M. Yamashita, *Nature Chem.* **2020**, *12*, 36; c) R. J. Schwamm, M. P. Coles, M. S. Hill, M. F. Mahon, C. L. McMullin, N. A. Rajabi, A. S. S. Wilson, *Angew. Chem. Int. Ed.* **2020**, *59*, 3928; d) K. Koshino, R. Kinjo, *J. Am. Chem. Soc.* **2020**, *142*, 9057; e) S. Grams, J. Eyselein, J. Langer, C. Färber, S. Harder, *Angew. Chem. Int. Ed.* **2020**, *59*, 15982; f) S. Grams, J. Mai, J. Langer, S. Harder, *Organometallics* **2022**, *41*, 2862; g) G. Feng, K. L. Chan, Z. Lin, M. Yamashita, *J. Am. Chem. Soc.* **2022**, *144*, 22662; h) C. Yan, R. Kinjo, *Angew. Chem. Int. Ed.* **2022**, *61*, e202211800; i) R. A. Jackson, A. J. R. Matthews, P. Vasko, M. F. Mahon, J. Hicks, D. Liptrot, *Chem. Commun.* **2023**, *59*, 5277.
[11] a) K. Hobson, C. J. Carmalt, C. Bakewell, *Chem. Sci.* **2020**, *11*, 6942; b) J. Hicks, P. Vasko, J. M. Goicoechea, S. Aldridge, *Angew. Chem. Int. Ed.* **2021**, *60*, 1702; c) M. P. Coles, M. J. Evans, *Chem. Commun.* **2023**, *59*, 503.
[12] J. Hicks, P. Vasko, A. Heilmann, J. M. Goicoechea, S. Aldridge, *Angew. Chem. Int. Ed.* **2020**, *59*, 20376.
[13] J. Hicks, P. Vasko, J. M. Goicoechea, S. Aldridge, *J. Am. Chem. Soc.* **2019**, *141*, 11000.
[14] a) T. X. Gentner, M. J. Evans, A. R. Kennedy, S. E. Neale, C. L. McMullin, M. P. Coles, R. E. Mulvey, *Chem. Commun.* **2022**, *58*, 1390; b) S. Banerjee, G. M. Ballmann, M. J. Evans, A. O'Reilly, A. R. Kennedy, J. R. Fulton, M. P. Coles, R. E. Mulvey, *Chem. Eur. J.* **2023**, *29*, e202301849; c) M. J. Evans, M. D. Anker, C. L. McMullin, S. E. Neale, M. P. Coles, *Angew. Chem. Int. Ed.* **2021**, *60*, 22289; d) M. J. Evans, S. E. Neale, M. D. Anker, C. L. McMullin, M. P. Coles, *Angew. Chem. Int. Ed.* **2022**, *61*, e202117396; e) H.-Y. Liu,

M. S. Hill, M. F. Mahon, C. L. McMullin, R. J. Schwamm, *Organometallics* **2023**, *42*, 2881.
[15] N. Villegas-Escobar, A. Toro-Labbé, H. F. Schaefer, *Chem. Eur. J.* **2021**, *27*, 17369.
[16] We note that the authors incorrectly assign this movement to the H2 centre ("H" in their nomenclature), stating "afterward when the Al–H' is almost formed, the remaining H atom follows a C-shaped trajectory toward the final Al–H formation. This observation is repeated in the mechanism from the respective TSs for the dimeric complex." We have provided a movie of the trajectory in the ESI to visualise this process.
[17] A. V. Protchenko, K. H. Birjkumar, D. Dange, A. D. Schwarz, D. Vidovic, C. Jones, N. Kaltsoyannis, P. Mountford, S. Aldridge, *J. Am. Chem. Soc.* **2012**, *134*, 6500.
[18] A. Hinz, F. Breher, *Angew. Chem. Int. Ed.* **2018**, *57*, 8818.
[19] M. Bursch, J.-M. Mewes, A. Hansen, S. Grimme, *Angew. Chem. Int. Ed.* **2022**, *134*, e202205735.
[20] B. Schirmer, S. Grimme, *Top. Curr. Chem.* **2013**, *332*, 213.
[21] X. Zhang, Z. Cao, *Dalton Trans.* **2016**, *45*, 10355.
[22] M. Xu, A. R. Jupp, Z.-W. Qu, D. W. Stephan, *Angew. Chem. Int. Ed.* **2018**, *57*, 11050.
[23] E. Kaufmann, S. Sieber, P. V. Ragué Schleyer, *J. Am. Chem. Soc.* **1989**, *111*, 121.
[24] R. C. Turnell-Ritson, J. S. Sapsford, R. T. Cooper, S. S. Lee, T. Földes, P. A. Hunt, I. Pápai, A. E. Ashley, *Chem. Sci.* **2018**, *9*, 8716.
[25] T. Özgün, K. Bergander, L. Liu, C. G. Daniliuc, S. Grimme, G. Kehr, G. A. Erker, *Chem. Eur. J.* **2016**, *22*, 11958.
[26] C. Lepetit, P. Fau, K. Fajerwerg, M. L. Kahn, B. Silvi, *Coord. Chem. Rev.* **2017**, *345*, 150.
[27] S. Grams, J. Mai, J. Langer, J. Langer, S. Harder, *Dalton Trans.* **2022**, *51*, 12476.
[28] a) T. X. Gentner, R. E. Mulvey, *Angew. Chem. Int. Ed.* **2021**, *60*, 9247; b) J. M. Gil-Negrete, E. Hevia, *Chem. Sci.* **2021**, *12*, 1982.

Manuscript received: January 10, 2025
Accepted manuscript online: January 16, 2025
Version of record online: February 3, 2025